Towards an Automated Segmentation of the Ventro-Intermediate Thalamic Nucleus

Elena Najdenovska[1,2(✉)], Constantin Tuleasca[3,4,5], João Jorge[1,6], José P. Marques[7], Philippe Maeder[2], Jean-Philippe Thiran[2,4], Marc Levivier[3,5], and Meritxell Bach Cuadra[1,2,4]

[1] Centre d'Imagerie BioMédicale (CIBM), University of Lausanne (UNIL), 1015 Lausanne, Switzerland
elena.najdenovska@unil.ch
[2] Department of Radiology, Lausanne University Hospital (CHUV) and University of Lausanne (UNIL), 1011 Lausanne, Switzerland
[3] Department of Clinical Neurosciences, Neurosurgery Service and Gamma Knife Center, Lausanne University Hospital (CHUV), 1011 Lausanne, Switzerland
[4] Signal Processing Laboratory (LTS5), École Polytechnique Fédérale de Lausanne (EPFL), 1015 Lausanne, Switzerland
[5] Faculty of Biology and Medicine, University of Lausanne (UNIL), 1015 Lausanne, Switzerland
[6] Laboratory for Functional and Metabolic Imaging, École Polytechnique Fédérale de Lausanne (EPFL), 1015 Lausanne, Switzerland
[7] Donders Center for Cognitive Neuroimaging, Radboud University, 6525 HP Nijmegen, The Netherlands

Abstract. The ventro-intermediate nucleus (Vim), as the others thalamic subparts, cannot be directly visualized by current standard magnetic resonance imaging (MRI), in daily clinical practice. Hence, for treatment of tremor in functional neurosurgery, where the commonly used target is the Vim, the targeting procedure is done indirectly. We present a novel direct automated segmentation of the Vim using only subject-related MRI information, specifically, diffusion MRI at 3T and susceptibility weighted images (SWI) acquired at 7T. With a state-of-the-art method based on local diffusion MR properties for automated subdivision of the thalamus, we first restrain the region of interest to the group of motor-related nuclei. Then, this thalamic part is further subdivided, in graph parcellation manner, using the intensity-related features provided by SWI together with prior knowledge of the Vim localization inside the motor thalamic segment. Our framework was tested in four healthy elderly subjects, for eight thalami in total, and the results were evaluated by an experienced neurosurgeon, showing the ability to directly detect the Vim area. The qualitative inspection indicated that the proposed method outperforms standard multi-atlas based techniques.

Keywords: Vim · Automated segmentation · 7T susceptibility weighted images

1 Introduction

The ventro-intermediate nucleus (Vim) is part of the motor-group of thalamic nuclei. Its major importance comes from being the most common target in functional neuro-surgery as a treatment for tremor, either in standard procedures (deep brain stimulation or radiofrequency thalamotomy) or in alternative minimally invasive therapies (Vim radiosurgery or High Intensity Focused Ultrasound) [1, 2]. However, due to the lack of intrinsic or inherent contrast inside the thalamic area, the Vim is not directly visible on standard magnetic resonance imaging (MRI) routinely used in daily clinical practice acquired from field up to 3T. Consequently, the targeting for drug-resistant tremor is done in an indirect way by employing stereotactic coordinates or quadrilatere of Guiot [3]. Such approaches are mainly built upon a statistical average over the population and therefore, lack in representation of the individual variability.

To address these limitations, several research groups have made an attempt for an automated parcellation of the thalamus mainly based on diffusion-weighted images (DWI) acquired at 3T with the purpose of exploring the fibers orientation within the thalamic subparts [4–8]. In this context, Battistella et al. [4] recently proposed a robust method that partitions the thalamus in seven groups of nuclei using the Orientation Distribution Functions (ODFs) expressed in the Spherical Harmonic (SH) Basis that is outperforming the most advanced diffusion features so far. One of the segmented clusters represents the ventro-lateral ventral (VLV) thalamic part i.e. the motor-related group of nuclei including the Vim. However, the Vim cannot be accurately depicted with diffusion MRI, for instance as a separate component of VLV, mainly due to the relatively low spatial resolution of the standard DWI ($\sim 2 \times 2 \times 2$ mm^3).

Advanced developments in MRI at ultra-high field (7T) provides not only better spatial resolution, but also an improved intensity-contrast variation inside the thalamus, namely with the susceptibility mapping approaches. Moreover, Abosch et al. have indicated the correspondence of the observed features on susceptibility-weighted imaging (SWI) acquired at 7T with the thalamic anatomy [9] and subsequently they suggested the possibility of a direct visualization of the Vim on those images. Nevertheless, while the subthalamic nucleus has been validated for 7T in a clinical frame, the Vim observations remain purely descriptive.
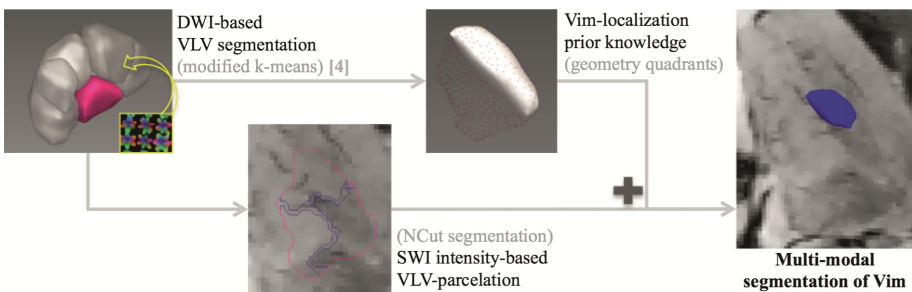

Fig. 1. Schematic overview of the proposed framework

The aim of this study is to automatically segment the Vim by combining SWI information at ultra-high field and prior knowledge of the VLV group of nuclei extracted from diffusion MRI. More specifically, we will combine NCut graph segmentation based on SWI intensity with a high-probability map of Vim localization derived from diffusion MRI thalamic clustering. Figure 1 shows a scheme of the proposed framework.

2 Materials and Methods

2.1 Dataset

The core of this study is performed in a dataset acquired at both 3 and 7T from four healthy elderly subjects (mean $\pm$ std: 67.2 ± 9.5 years, 3 males). Additional data from four healthy young subjects (28.5 ± 2.6 years, 2 males), for whom manual delineation of the Vim is available, was used for building atlases for comparison purposes. None of the subjects had any particular neurological disease nor a brain deformation caused by intracranial lesions. The study was approved by the local institutional review board and an informed consent was obtained from all the participants.

Image Acquisitions. The data from elderly subjects at 3T was acquired with a Prisma Siemens scanner and it included a T1-weighted (T1w, MPRAGE) sequence (TR/TE = 2300/2.03 ms, TI = 900 ms, voxel size: 1 mm^3) and DWI (64 gradient directions, b = 1000 s/mm^2, TR/TE = 7100/84 ms, voxel-size: $2.24 \times 2.24 \times 2.2$ mm^3). T1w images from the healthy population were acquired with 3T TIM Trio Siemens scanner with similar acquisition parameters as those for the elderly population.

For all eight subjects, the ultra-high field data was acquired with a 7T, 68 cm-*wide bore* MRI system from SIEMENS Medical Solutions, equipped with a single-channel transmit/32-channel receive head RF array (Nova Medical). This data included axial SWI (with a restrained field of view, FoV, surrounding the thalamus, TR/TE = 28/20 ms, flip-angle 10°, voxel-size: $0.375 \times 0.375 \times 1$ mm^3, 72 slices) and T1w (MP2RAGE) sequence (TR/TE = 6000/2.05 ms, TI$_1$/TI$_2$ = 800/2700 ms, flip-angles: 7/5°, voxel-size: $0.6 \times 0.6 \times 0.6$ mm^3).

Common Image Space. We choose to work in the individual anterior commissure-posterior commissure (AC-PC) image space of each elderly subject. The image space was defined by the T1 template in MNI space of voxel size $0.5 \times 0.5 \times 0.5$ mm^3 [10] whose AC-PC plane was aligned horizontally. Each 3T MPRAGE was transformed into this AC-PC space by a rigid transform, and the individual resulting image, *T1w_acpc*, was considered as reference for the successive image transformations described in the following sections.

2.2 Thalamic Parcellation

The preprocessing of the DWI included several steps: data denoising [11, 12], bias field [13, 14], motion [15] and eddy current corrections [16]. Furthermore, with a non-linear registration, using FSL's FNIRT [13], between the T1w_acpc and the respective

fractional anisotropy (FA) map, we compensated the EPI distortions presented in the DWI data. On the preprocessed data we performed the Q-ball fitting of the Constant Solid Angle ODFs (FSL qboot) with maximum SH order of 6, accordingly to [4].

The thalamus masks were obtained from the FreeSurfer's subcortical parcellation, performed for each 3T MPRAGE, and further refined, as described in [4], by automatically removing voxels with FA value greater than 0.55 and celebro-spinal fluid's probability exceeding 5%. Subsequently to a qualitative comparison between the refined masks and the SWI where the thalamic borders appear more discernible, missing voxels were manually added mainly in the anterior and the lateral part of the inferior thalamic slices.

Following the framework description in [4], the thalamus was subdivided in 7 clusters while applying a modified k-means using as features the spatial position of the thalamic voxels and the corresponding ODF coefficients in the SH basis. The obtained results, including the VLV cluster were then brought in the AC-PC space by applying the non-linear transform, as described earlier, matching the FA and T1w_acpc image.

2.3 The Proposed Framework

The VLV cluster, other than Vim, includes several motor-related nuclei. However, in correspondence to the findings described in [9], in SW imaging, the ventral nuclei surrounding the Vim, such as ventro-caudalis (Vc) and ventro-odalis (Vo), appear as darker regions in comparison with our area of interest (see Fig. 2). These contrast differences we observed inside the VLV drove us to explore the SWI-intensity for a further VLV subdivision aiming towards an automated delineation of the Vim.
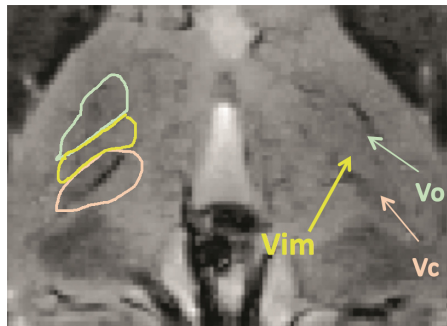

Fig. 2. Illsutration of the SWI visible structures surrounding the Vim in axial view. On the right side we have manually in-plane draw of the visible ventral nuclei in correspondence with the Schaltenbrand and Wahren atlas [17], while on the left they are indicated with arrows. The yellow represents the Vim, while the bright green and the bright orange ventro-caudalis (Vc) and ventro-odalis (Vo), which are surrounding the Vim as darker areas. (Color figure online)

SWI Preprocessing. The SWI images from our elderly cohort were corrected for intensity inhomogeneities using the N4ITK bias field correction algorithm [18]. The obtained images were first registered to the corresponding 7T MP2RAGE with a rigid

transform and then brought to the AC-PC space by applying the analogous affine transform that matched the 7T MP2RAGE and T1w_acpc.

Primary analysis of the SWI data showed high intensity variability among the subjects and different head position in the scanner. Therefore, to standardize the image intensity appearing on these images, we applied the histogram equalization algorithm proposed by Nyul et al. [19] that represents an one-to-one image transformation and therefore, does not affect the image appearance. We work in a volume of interest (VOI) surrounding both thalami for each subject respectively. Figure 2 is representing an axial slice of the used VOI in one case. All four SWI images from the elderly population were used in the training step where the standard scale was build upon the deciles extracted from each image histogram. The results from this histogram matching are shown in Fig. 3.
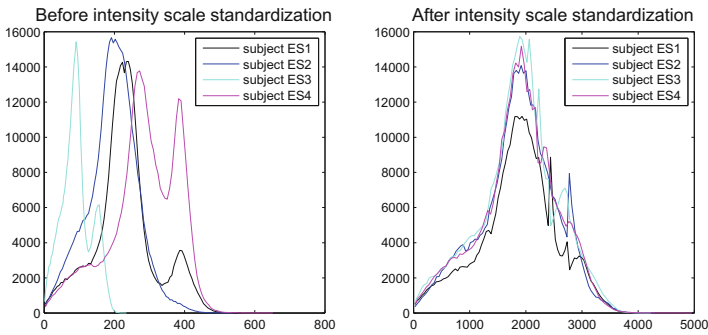

Fig. 3. Histogram equalization of the SWI intensity inside the thalamic area

To further enhance the edges and observable features on the SWI, the ITK gradient anisotropic diffusion filtering of conductance 0.3 was applied.

Graph Representation and Parcellation. The preprocessed SWI-intensity information inside the VLV was transformed in a graph representation of the data. More precisely, we constructed a k-nn graph with 50 nearest neighbors, where the edges' weights expressed the Gaussian weighting of the linear combination between the intensity distance (*Dint*) and the Euclidean distance among the VLV voxels (*Dpos*):

$$D = Dint + \gamma Dpos \tag{1}$$

where γ represents the ratio between *max(Dint)* and *max(Dpos)* and therefore, it acts as a scaling factor that brings the *Dpos* in the same range of values as *Dint*.

The parcellation of the graph was performed with Normalized Cut (NCut) partition [20]. We subdivided the VLV in 3 sub-clusters. The number 3 was chosen empirically since it gives a consistent parcellation pattern corresponding to our prior knowledge/ hypothesis of the VLV structure: the region with bright SWI intensity as the expected one in the Vim area, the region with darker SWI intensity and an auxiliary part (see Fig. 4B1).
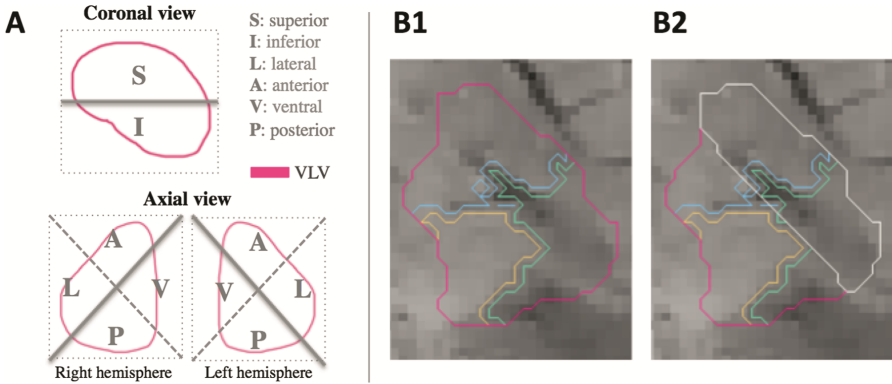
Fig. 4. Isolation of the inferior anterio-lateral part of the VLV cluster. Panel A shows a schematic illustration of the VLV-cluster separation in 8 geometrical quadrants, while panel B shows a real-case example of the left VLV in axial view. In panel B1 the diffusion-based VLV outline is given with the magenta contour and additionally we can observe the three parcels obtained from SWI intensity-based NCut partition. The VLV_ial part for the given case is shown with the white contour in panel B2. (Color figure online)

Geometry Quadrants. To isolate the inferior anterio-lateral part of the VLV cluster obtained from diffusion MRI (Sect. 2.2), *VLV_ial*, where the Vim is most likely to be found, we proceeded at dividing the VLV using the geometry of the smallest rectangular cuboid that contains all of its non-zero voxels. In fact, with the cuboid's mid-plane, we separated the inferior from the superior part and with the in-plane diagonals the anterio-lateral from the ventral-posterior part (see Fig. 4A).

The separated VLV_ial portion was used to confine the NCut parcellation to the expected localization of the Vim (Fig. 4B).

2.4   Multi-atlas Segmentation

In this work we propose a direct segmentation of the Vim by using subject specific information from both diffusion MRI and SWI. The state-of-the-art lacks in Vim-delineation approaches. However, if an atlas is available, this could be achieved with the atlas-based segmentation techniques. Hence, we additionally aim at performing a multi-atlas based segmentation and comparing it to the outcome of our multi-modal framework. As atlases we used SWI data from young subjects where the Vim was manually delineated by an experienced neurosurgeon. The manual delineation was mainly based upon the visible contrast variation together with the observation shown in [9] and the Schaltenbrand and Wahren atlas [17].

For transforming the atlases in each respective AC-PC space previously defined, our initial attempt was to directly match the SWIs but, presumably due to the variation of the FoV orientation among the subjects, all image registration technics failed to provide a good matching. Therefore, the atlases correspondence was done via the T1w images, by calculating consecutively linear and BSpline transform between the respective atlas' 3T MPRAGE and the T1w_acpc. The final multi-atlas outline was obtained by applying

the Joint Label Fusion method with corrective learning [21] within the thalamic VOI previously defined.

3   Results

The proposed framework was tested for the group of elderly subjects or, more precisely, eight thalami in total. The intersection between the NCut parcellation and the VLV_ial portion mainly resulted in two subdivisions. Among the two, we choose as Vim outline the region showing brighter intensity (see Fig. 4 panel B). As described in Sect. 2.4, atlas-based segmentation using 4 thalami per hemisphere was also performed.

The multi-atlas outline represented in general smaller area than the multi-modal outline. However, overlap between both delimitations was always observed. Additionally, for six out of eight thalami, the major part of the multi-atlas Vim delimitation was inside the one from the multi-modal segmentation. For the remaining two cases, a blood vessel was observed in the targeted area disintegrating its intensity homogeneity (Fig. 5, right hemisphere of ES2 and ES4). Overall results are illustrated in Fig. 5.
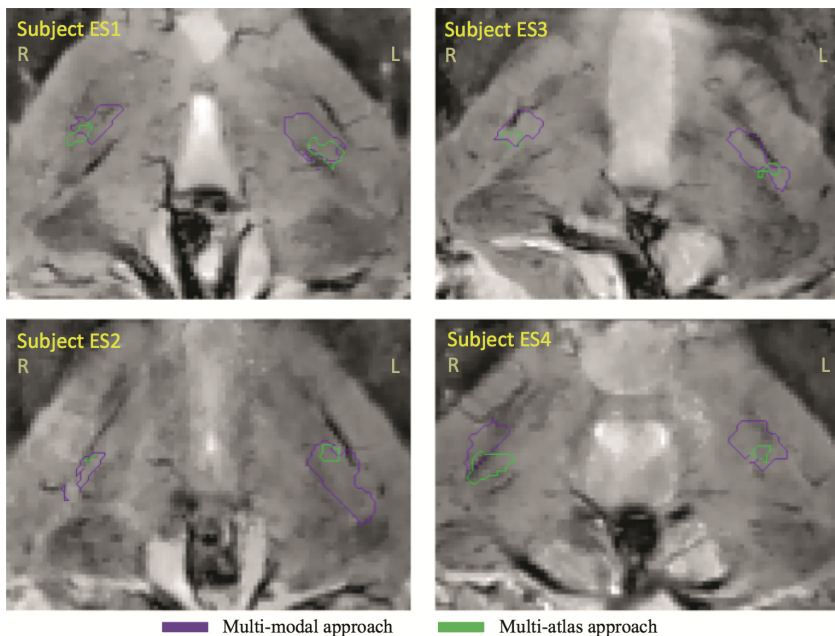

Fig. 5. Visual overview of the obtained findings for each tested subject respectively in an axial slice. The multi-modal outline corresponds to the violet contour, while the multi-atlas one to the green contour. (Color figure online)

The results provided by the proposed framework were qualitatively validated by the same neurosurgeon who did the manual delimitation of the Vim in the atlases. His observations were that, despite the tendency of the multi-modal approach to do a slight

overestimation of the visually expected Vim extend by enclosing minor parts of the surrounding thalamic structures, they however portray more completely the region of interest than the small volumes provided by the multi-atlas approach. Additionally, the multi-modal delimitations are more consistent in symmetry over the hemispheres than the multi-atlas ones.

In the context of the size, the visual observations were confirmed with the calculated volumes of both multi-modal and multi-atlas segmentations given in Table 1. Since the expected size of the Vim is between 60 to 150 mm^3 [22], the volumes of the proposed multi-modal delimitation are sometimes marginally exceeding the expected range. In contrast to this, the multi-atlas delineations are importantly underestimating the size of the Vim.

Table 1. Volumes of the resulting Vim outlines

VOLUME [mm^3]	Multi-modal segmentation		Multi-atlas segmentation	
	Left	Right	Left	Right
Subject ES1	122.5	149.2	21.4	18.7
Subject ES2	196	54.7	14.7	29.7
Subject ES3	198.4	187.2	11.7	35
Subject ES4	176.1	129.2	5.4	29.1

4 Discussion

Although performed on a limited number of subjects, the present study represents an important step towards an automated segmentation of the Vim area. We used local diffusion MR properties inside the thalamus for delimitation of an initial region of interest, the VLV cluster enclosing the motor-related thalamic nuclei, which was further subdivided using the 7T SWI intensity and a prior knowledge of the Vim localization within the VLV. We additionally examined the ability of multi-atlas based techniques to segment the Vim.

The spatial distribution and extent of the resulting Vim outlines were qualitatively validated by an experienced neurosurgeon. A minor affinity of slightly imprecise borders regarding the surrounding structures was observed in the outcome of the proposed multi-modal method. Nevertheless, these outlines represent better and in more complete manner the Vim area than the limited extents provided by a multi-atlas segmentation approach. Analogue to this are the calculated volumes of the outlines.

The DWI used for the VLV delineation has approximately five times lower spatial resolution than the image reference space where the analysis were performed ($2.24 \times 2.24 \times 2.2$ mm^3 versus $0.5 \times 0.5 \times 0.5$ mm^3). As consequence we are prone to imprecise border delineation of the initial region of interest i.e. the VLV thalamic part. Another limitation comes from the non-robust contrast variation observed on the SWI together with the presence of the blood vessels in an indiscriminate mode, inside the VLV and the thalamus in general, increasing the potential of Vim's border inaccuracy. This could also have a major impact on direct visualization in some cases. Further studies should be done to understand the origin of the differences in feature appearance observed

on SWI for the populations of different age. We believe that standardization of the SWI contrast could make this imaging method even more powerful tool for direct visualization, especially for direct targeting in functional neurosurgery in drug-resistant tremor.

In this study we have also shown that the imaging method based on the individual subjects' anatomy outperforms the approaches build from statistical average among a chosen population, such as the atlases. As limitation of the used multi-atlas approach we consider the image registration done between the respective T1w images on which the thalamus appears as a homogeneous area with borders that are difficult to discriminate. Hence, the information provided for the thalami matching and the corrective learning afterwards is not optimal. Possible improvement in this context could be the direct use of the SWI for the image matching procedure, since it provides much more features of the thalamic architecture. However, mainly due to the variation of the SWI FoV orientation, it was difficult to achieve such task in the presented data.

The proposed multi-modal framework should be further quantitatively evaluated against a manual delamination of the targeted area. Nevertheless, it represents a novel advancement in the field of automated subject-specific segmentation of the Vim.

References

1. Lipsman, N., Schwartz, M.L., Huang, Y., Lee, L., Sankar, T., Chapman, M., Hynynen, K., Lozano, A.M.: MR-guided focused ultrasound thalamotomy for essential tremor: a proof-of-concept study. Lancet Neurol. **12**, 462–468 (2013)
2. Witjas, T., Carron, R., Krack, P., Eusebio, A., Vaugoyeau, M., Hariz, M., Azulay, J.P., Regis, J.: A prospective single-blind study of Gamma Knife thalamotomy for tremor. Neurology **85**, 1562–1568 (2015)
3. Kondziolka, D., Ong, J.G., Lee, J.Y., Moore, R.Y., Flickinger, J.C., Lunsford, L.D.: Gamma Knife thalamotomy for essential tremor. J. Neurosurg. **108**, 111–117 (2008)
4. Battistella, G., Najdenovska, E., Maeder, P., Ghazaleh, N., Daducci, A., Thiran, J.P., Jacquemont, S., Tuleasca, C., Levivier, M., Bach Cuadra, M., Fornari, E.: Robust thalamic nuclei segmentation method based on local diffusion magnetic resonance properties. Brain Struct. Funct. (2016)
5. Behrens, T.E., Johansen-Berg, H., Woolrich, M.W., Smith, S.M., Wheeler-Kingshott, C.A., Boulby, P.A., Barker, G.J., Sillery, E.L., Sheehan, K., Ciccarelli, O., Thompson, A.J., Brady, J.M., Matthews, P.M.: Non-invasive mapping of connections between human thalamus and cortex using diffusion imaging. Nat. Neurosci. **6**, 750–757 (2003)
6. Mang, S.C., Busza, A., Reiterer, S., Grodd, W., Klose, A.U.: Thalamus segmentation based on the local diffusion direction: a group study. Magn. Reson. Med. **67**, 118–126 (2012). Official Journal of the Society of Magnetic Resonance in Medicine/Society of Magnetic Resonance in Medicine
7. Wiegell, M.R., Tuch, D.S., Larsson, H.B., Wedeen, V.J.: Automatic segmentation of thalamic nuclei from diffusion tensor magnetic resonance imaging. NeuroImage **19**, 391–401 (2003)

8. Ziyan, U., Tuch, D., Westin, C.-F.: Segmentation of thalamic nuclei from DTI using spectral clustering. In: Larsen, R., Nielsen, M., Sporring, J. (eds.) MICCAI 2006. LNCS, vol. 4191, pp. 807–814. Springer, Heidelberg (2006). doi:10.1007/11866763_99

9. Abosch, A., Yacoub, E., Ugurbil, K., Harel, N.: An assessment of current brain targets for deep brain stimulation surgery with susceptibility-weighted imaging at 7 tesla. Neurosurgery **67**, 1745–1756 (2010). Discussion 1756

10. Fonov, V.S., Evans, A.C., McKinstry, R.C., Almli, C.R., Collins, D.L.: Unbiased nonlinear average age-appropriate brain templates from birth to adulthood. NeuroImage **47**(Supplement 1), S102 (2009)

11. Tournier, J.D., Calamante, F., Connelly, A.: MRtrix: diffusion tractography in crossing fiber regions. Int. J. Imaging Syst. Technol. **22**, 53–66 (2012)

12. Veraart, J., Novikov, D.S., Christiaens, D., Ades-Aron, B., Sijbers, J., Fieremans, E.: Denoising of diffusion MRI using random matrix theory. NeuroImage **142**, 394–406 (2016)

13. Smith, S.M., Jenkinson, M., Woolrich, M.W., Beckmann, C.F., Behrens, T.E., Johansen-Berg, H., Bannister, P.R., De Luca, M., Drobnjak, I., Flitney, D.E., Niazy, R.K., Saunders, J., Vickers, J., Zhang, Y., De Stefano, N., Brady, J.M., Matthews, P.M.: Advances in functional and structural MR image analysis and implementation as FSL. NeuroImage **23**(Suppl 1), S208–S219 (2004)

14. Zhang, Y., Brady, M., Smith, S.: Segmentation of brain MR images through a hidden Markov random field model and the expectation-maximization algorithm. IEEE Trans. Med. Imaging **20**, 45–57 (2001)

15. Leemans, A., Jones, D.K.: The B-Matrix must be rotated when correcting for subject motion in DTI Data. Magn. Reson. Med. **61**, 1336–1349 (2009)

16. Andersson, J.L., Sotiropoulos, S.N.: An integrated approach to correction for off-resonance effects and subject movement in diffusion MR imaging. NeuroImage **125**, 1063–1078 (2016)

17. Schaltenbrand, G., Wahren, W.: Atlas for Stereotaxy of the Human Brain. Year Book Medical Publishers (1977)

18. Tustison, N.J., Avants, B.B., Cook, P.A., Zheng, Y.J., Egan, A., Yushkevich, P.A., Gee, J.C.: N4ITK: improved N3 bias correction. IEEE Trans. Med. Imaging **29**, 1310–1320 (2010)

19. Nyul, L.G., Udupa, J.K., Zhang, X.: New variants of a method of MRI scale standardization. IEEE Trans. Med. Imaging **19**, 143–150 (2000)

20. Shi, J.B., Malik, J.: Normalized cuts and image segmentation. In: Proceedings of CVPR IEEE, pp. 731–737 (1997)

21. Wang, H., Yushkevich, P.A.: Multi-atlas segmentation with joint label fusion and corrective learning-an open source implementation. Front. Neuroinform. **7**, 27 (2013)

22. Tuite, P.J., Dagher, A.: Magnetic Resonance Imaging in Movement Disorders: A Guide for Clinicians and Scientists. Cambridge University Press, Cambridge (2013)